

ASSESSMENT OF THICKENED FLAME MODEL COUPLED WITH FLAMELET GENERATED MANIFOLD ON A LOW-SWIRL PARTIALLY PREMIXED GASEOUS LIFTED FLAME

Leonardo Langone*
Matteo Amerighi
Lorenzo Mazzei
Antonio Andreini

Heat Transfer and Combustion group
Department of Industrial Engineering
via di Santa Marta, 3, Florence, 50139, Italy

Stefano Orsino
Naseem Ansari
Rakesh Yadav
ANSYS, Inc.
United States

ABSTRACT

The present work focuses on the numerical modeling through Large Eddy Simulations (LES) of a low-swirl partially premixed lean flame operated with gaseous fuel using a hybrid Thickened Flame (TF)-Flamelet Generated Manifolds (FGM) combustion model. This approach aims to overcome the challenges of modeling the flame lift-off in this burner and the stabilization of the reaction zone at a remarkable distance from the nozzle outlet section, for which the reproduction of finite rate effects on combustion physics is crucial. The underlying strategy consists of applying the artificial thickening to the scalar equations required for the query of the look-up table computed a priori. The mentioned combustion model has been implemented in a general-purpose commercial CFD solver and Non-Adiabatic Flamelets have been employed for the look-up table computation. The goal is to include a detailed chemistry description while maintaining a cost-effective approach and improving the reproduction of the turbulence-chemistry interaction. Results are validated with experimental data in terms of temperature and chemical species concentration maps, showing the potential of the coupled TF-FGM approach for describing this type of flame.

*Address all correspondence to this author: leonardo.langone@unifi.it

NOMENCLATURE

c	Progress variable	[-]
s_l	Laminar flame speed	[m/s]
Y	Mass fraction	[m/s]
z	Mixture fraction	[-]
h	Enthalpy	[kJ/kg]
ϕ	Equivalence ratio	[-]
$\dot{\omega}$	Reaction rate	[kg/m ³ s]
δ	Flame thickness	[m]
S	Swirl Number	[-]

Subscripts

ad	Adiabatic
$theo$	Theoretical
th	Thermal

Acronyms

CFD	Computational Fluid Dynamics
FGM	Flamelet Generated Manifold
IRZ	Inner Recirculation Zone
LDA	Laser Doppler Anemometry
LES	Large Eddy Simulation
LOH	Lift-off height
ORZ	Outer Recirculation Zone
PDF	Probability Density Function
TF	Thickened Flame

INTRODUCTION

Low Swirl combustion has been widely investigated for its potential in terms of reduction of nitrogen oxides (NOx) emissions and resistance to flashback occurrence [1]. These advantages are related to the flame assuming a lifted configuration, which means that it is detached from the nozzle exit and stabilized downstream in the chamber. Among the several investigations concerning this type of combustion [2, 3], one of the most interesting for the gas turbine's application field has been carried out at the Engler Buntler Institute (EBI) of the Karlsruhe Institute of Technology (KIT) recently [4,5]. Here, a specific injector with separate inlets for air and fuel was used, which classifies this system as a non-premixed one. However, as highlighted during the experimental campaigns, the premixing process for the reactive mixture occurs in the lift-off region, and finally a *premixed-like* regime is achieved. Although this burner has been largely investigated through experiments, Computational Fluid Dynamics (CFD) could help to extend the knowledge about this flame to a wider set of operating conditions and burner configurations. Moreover, scale resolving methods, such as Large Eddy Simulation (LES), have been demonstrated to be a proper tool for investigating the reactive process [6, 7]. However, the numerical modeling of a lifted flame remains extremely challenging due to the high degree of complexity of the physics involved in the lift-off occurrence [8], where a correct reproduction of the finite rate effects is mandatory since they control the ignition of the fresh mixture and thus the stabilization of the flame.

In the years, several modelling strategies have been proposed from the scientific community to this aim. Flamelet-based approaches [9–12] have become quite popular in the engineering community since their capability to represent the flame gathered with appreciable cost-effectiveness in terms of computational efforts. On the other hand, the limitations of a priori regime assumption and chemistry tabulation could strongly impact the final prediction [13], and nowadays many research efforts are devoted to compare finite rate methods with and flamelets-based ones for describing turbulent combustion [14, 15].

Considering the numerical works carried out so far on the KIT-EBI's flame [16, 17], turbulent combustion has been initially modeled with flamelets based approaches as (or very similar to) the Flamelet Generated Manifold (FGM). This model however has shown to overpredict the reaction rate, leading to a flame stabilized too low and short with respect to the experimental finding. The prediction can be improved when the FGM model is modified to take into account the effects of local stretch and heat loss on the global reactivity, referred as FGM-EXT in [17]. Further works from the authors [18] carried out a comparison among the previously mentioned models and the Thickened Flame (TF) model [19]: indeed, the use of the TF approach resulted in a better description of the flame lift-off and shape of the reaction zone. However, this first attempt employed the BFER 2-step mechanism by Franzelli et al. [20] for the chemistry description, which

is not adequate to quantitatively describe intermediate species such as carbon monoxide (CO) [21]. The use of a more detailed mechanism seemed to be preferable to catch properly the lift-off while retrieving information on intermediate species [22] but it will lead to very expensive calculations in terms of computational efforts. A possible strategy to improve the accuracy of the numerical prediction, while keeping a moderate computational cost is represented by the use of coupled TF-FGM approach, where the artificial thickening is applied to the scalar reactive quantities employed in the manifold parametrization. This approach has been already proposed [23] and successfully applied [24–26] in the literature, showing to be able to achieve both the mentioned goals. Moreover, Proch et al. in [27] highlighted the importance of heat losses inclusion within the look-up table computation.

The goal of the present work is therefore to investigate how the flame prediction concerning the KIT-EBI's burner is affected when turbulence-chemistry interaction is described through the use of Thickened Flame model with a chemistry tabulation from a non-adiabatic FGM manifold. To some extent, this work represents a continuation of the study in [18], where all the employed models have been found not fully satisfactory with respect to the experimental data. The expected outcomes are to extend the knowledge concerning this type of low-swirl lifted flame, other than highlighting the possible advantages of this approach for industrial applications. To this aim the mentioned approach is implemented in the commercial code ANSYS Fluent with two different strategies to compute the velocity fluctuations for the efficiency function related to the flame wrinkling effects. The paper is structured as follows: firstly, the test case is described together with an overview of the low swirl partially premixed lifted flame features. Therefore, the employed combustion models are reported, especially concerning the strategy used within the coupling procedure. Finally, the numerical simulations are compared with the available experimental data in terms of chemical species and temperature fields. Some final remarks are drawn concerning the substantial advantage of the TF-FGM approach with respect to the standard FGM, as a suitable model to investigate this type of lifted flame also in more complex configurations (e.g., multiburner arrangement).

TEST CASE AND FLAME FEATURES

The burner employed in the studies by Fokaides and coworkers [4, 5] is considered. This flame consists of a partially premixed flame operated with gaseous fuel. The experimental campaign aimed to investigate the stability of such flame and the parameters which influence the reaction zone position and extension. The flame lift-off is due to the use of a low swirl injector, where the overall theoretical Swirl Number $S_{theo} = \dot{D}_i/R_i\dot{I}_i$ is below 0.4, being the ratio between the angular to the axial flux momentum divided by the narrowest radius of each channel. The

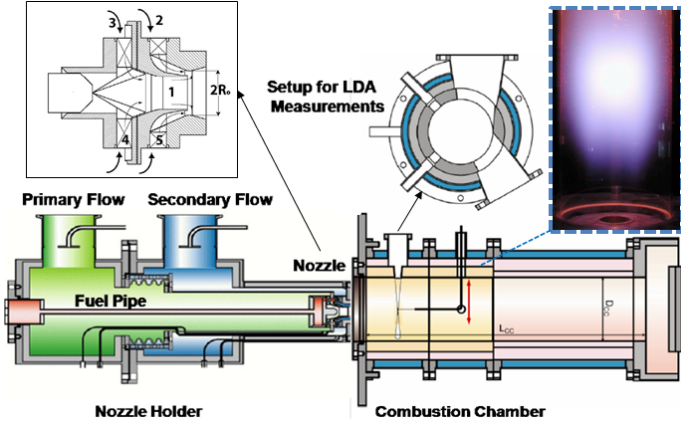


FIGURE 1: SKETCH OF THE TEST RIG ADAPTED FROM [4].

injector is derived from an air-blast atomizer [28], then modified to replace the liquid fuel with methane. This adopts a double-swirled radial configuration where $S_{theo} = 0.76$ and $S_{theo} \approx 0.0$ (i.e., no swirl component in the flow) respectively for the primary channels and the second ones. Its characteristic is the presence of a high-velocity swirling jet issuing from the nozzle, where the Inner Recirculation Zone (IRZ) is relatively weak and enveloped within the high-velocity jet streams. The Outer Recirculation Zone (ORZ) due to the interaction between the swirling jet and the chamber walls has great relevance since it plays a major role in the transport of hot combustion products from the main reaction zone to the base of the flame. Actually, according to the experimental investigators, the flame cannot be ignited without the presence of the confinement wall, since this zone could not be established [5]. The flame is anchored on the outer shear layer of the swirling jet and stabilizes in a region where the mixing process has concluded, obtaining premixed-like combustion conditions. Furthermore, the experimental studies agreed on the role played by the recirculating gas temperature as responsible for the ignition of the fresh mixture, thus the flame stabilization [4]. Indeed, heat losses through the confinement walls decrease the recirculating gas temperature and thus delay the reactive mixture ignition, finally increasing the lift-off height.

The test rig considers a cylindrical combustion chamber with a diameter D_{CC} of four times the throat diameter of the nozzle diffuser $2R_0$. The outlet section is placed at a distance L_{CC} corresponding to four and half times D_{CC} from the chamber bottom, with the outlet geometry specifically designed to avoid back-flow recirculation. The burner operates at atmospheric pressure and the main section consists of a ceramic segment with water cooling, while different additional segments can be employed allowing the specific measurement techniques. Flow-field measurements have been obtained with Laser Doppler Anemometry (LDA) technique, when optical access is provided. Local species concentration in the combustion chamber has been mea-

sured through gas sampling with a suction probe, then analyzed with conventional gas analyses based on molecular excitation process. Temperature measurements are also available thanks to S type compensated micro thermocouple probes corrected for radiative heat losses. A sketch of the test rig comprehensive of the measurements segments is reported in Fig.1. The test point considered in the present work employs methane as fuel and the associated operating conditions are reported in Tab.1, where lean global equivalence ratio $\phi = 0.65$ is considered for the present investigation.

Operating pressure p_0	101325 Pa
Air inlet temperature T_0	373 K
Air mass flow \dot{m}_{air}	0.0185 kg/s
Nozzle pressure drop $\Delta p_{nozzle}/p_0$	2 %
Equivalence ratio ϕ	0.65

TABLE 1: OPERATING CONDITIONS ADOPTED IN THE NUMERICAL SIMULATIONS.

COMBUSTION MODELLING

The present numerical investigation has been carried out in the CFD suite ANSYS Fluent 2021R2, where the TF-FGM approach was implemented for this investigation: in the followings, the modelling strategies are described and discussed.

Non Adiabatic Flamelet Generated Manifold (NFGM)

The FGM approach [11, 29] has become very popular in the engineering community since its cost-effectiveness while including a detailed chemistry description. The fundamental assumption is that combustion occurs in flamelet combustion regime, where the flame front is only wrinkled by the turbulence and it could be represented locally by laminar 1D flames [30]. At pre-process, a look-up table is generated by solving several flamelets and the associated thermochemical trajectories are stored as a function of two variables, the mixture fraction z (as defined by Bilger [31]) and the progress variable c . The latter is defined in this work as $c = Y_c/Y_c^{eq}$, where $Y_c = Y_{CO} + Y_{CO_2}$ is the un-normalized progress variable and Y_c^{eq} is its value at equilibrium. The turbulence-chemistry interaction is modeled with a pre-integration with presumed β -shaped Probability Density Functions (β -PDF). This means that the turbulent combustion is resolved considering only four additional variables, which are the mean values of the scalar and their respective variances (i.e., \tilde{z} , \tilde{c} , \tilde{z}''^2 , \tilde{c}''^2). In the literature various approaches have been

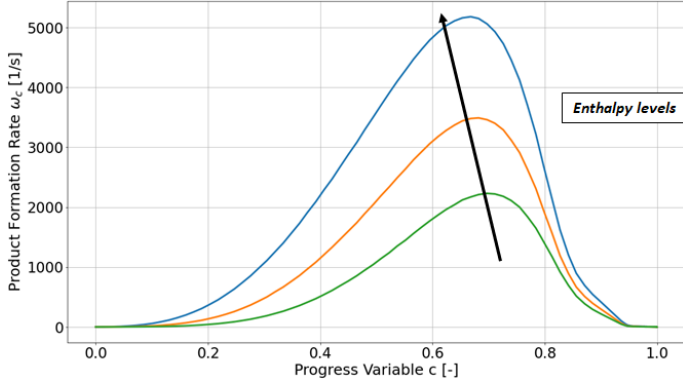


FIGURE 2: PRODUCT FORMATION RATE (I.E., PROGRESS VARIABLE REACTION RATE) VERSUS PROGRESS VARIABLE FOR VARIOUS ENTHALPY LEVELS ($\phi = 1.0$, AMBIENT PRESSURE AND INLET TEMPERATURE).

proposed to include heat losses effects as well as the actions of strain on the flame front [32–35], by increasing the dimension of the manifold: these often differ on how the heat loss is modeled in the flamelet, and a detailed description of the implications of each strategy can be found in [36].

In the previous works by the authors, the effects of heat losses were included within the FGM model through a correction factor applied by scaling the reaction rate [17, 18]: outcomes have shown a discrepancy with the experimental measurements, resulting in a short flame stabilized low in the flame tube. A possible explanation for such behaviour could be incorrect modelling of the heat loss effects on the reaction, due to this simplistic approach, as described in [35]. For this reason, here heat loss effects are taken into account during the look-up table generation thanks to the use of non-adiabatic flamelets. Indeed, the usual adiabatic flamelets do not consider the effect of enthalpy on the reaction, and these effects are handled only in the calculation by varying the temperature or gas properties. Instead, the use of non-adiabatic flamelets takes into account enthalpy loss or gain also during the generation of the table, therefore on the chemical species and related reaction rates. An example of the effect of enthalpy loss on the reaction rate is depicted in Fig.2 for given conditions.

In this work, the strategy adopted in the CFD code ANSYS Fluent 2021R2 [37] is used. Both freely propagating premixed flamelets for low values of heat loss and burner stabilized flamelets at higher levels are employed. These latter types introduced enthalpy loss or gain by varying the burner temperature [32]. The switch from one type of flamelet to another is done automatically based on inlet composition and enthalpy inlet at boundaries. The final table is a five-dimension manifold, where only an additional input for the enthalpy loss, since it is

convoluted in the table assuming a delta function. In this fashion, the overall cost-effective approach in terms of computational efforts is maintained. This new strategy has been validated for some well-known test cases in the literature [38], obtaining very interesting results. For the sake of clarity, the same nomenclature of [38] is used here, therefore the FGM model with non-adiabatic manifold is referred as NFGM in the next sections.

Aiming to compare the effects of this further tabulation with the previous works, the same settings of the table have been employed. It is worth recalling that the use of premixed flamelets is justified in relation to the premixed operating conditions reported from the experimental investigators, as mentioned earlier. The GRI3.0 detailed mechanism with 325 reactions and 53 species is used for the table computation. The table is discretized with 64×32 points in terms of respectively z and c . Instead, 21 levels are employed for the enthalpy loss/gain discretization. Also, the Finite Rate closure is employed for the progress variable source term modeling.

Coupled Thickened Flame-Flamelet Generated Manifold model (TF-FGM)

The focus of this work consists of applying the same artificial thickening used in the standard TF model [19] to the equation of the scalars from the FGM approach. In the TF model, the flame front is artificially thickened in order to be resolved on the usually employed mesh grid sizing. Indeed, from the dimensional analysis conducted in [39], the laminar flame speed s_l and the laminar flame thickness δ_l are proportional to $s_l \propto \sqrt{D_{th} \bar{\omega}_l}$ and $\delta_l \propto \sqrt{D_{th} / \bar{\omega}_l}$ respectively. Therefore, it is possible to artificially thicken the flame, preserving the correct laminar flame speed, by increasing the thermal diffusivity and decreasing proportionally the reaction rate through the introduction of a thickening factor $F = N\Delta/\delta$, where N is the number of points in the flame front (here set to 4), Δ is the mesh grid size and the laminar flame thickness δ . In this fashion, the correct laminar flame speed is preserved. Such operation however affects the interaction between chemistry and turbulence since the eddies are smaller than the thickened front are not interacting properly with the flame [30] and for this reason the reaction rates and the thermal diffusivity are multiplied by the efficiency function E , that will be discussed in the next section. Moreover, erroneous mixing related to the thickening procedure is avoided by applying the thickening dynamically only in the proximity of the flame front, through the use of a flame sensor Ω , assuming its value equal to 1 in the regions of interest and 0 away from them, as reported in [40]. Therefore, the source term in the progress variable equation is recast as follows:

$$\bar{\omega}_{c,TF} = \frac{E}{F} \bar{\omega}_{c,l} \quad (1)$$

being $\bar{\omega}_c, l$ is the mean source term of the progress variable provided by the PDF table, while the diffusivity is:

$$D_{eff} = D_l(1 + (EF - 1)\Omega) + D_t(1 - \Omega) \quad (2)$$

where D_l is the laminar diffusivity and D_t is the turbulent one. The final equation for the progress variable reads:

$$\frac{\partial \bar{\rho} \tilde{c}}{\partial t} + \frac{\partial \bar{\rho} \tilde{u}_j \tilde{c}}{\partial x_j} = \frac{\partial}{\partial x_j} \left(\bar{\rho} D_{eff} \frac{\partial \tilde{c}}{\partial x_j} \right) + \bar{\omega}_{c,TF} \quad (3)$$

For the sake of brevity, the mixture fraction z and the enthalpy h equations are not reported, considering that the whole procedure is applied in the exact same way to terms in the respective equations. An important point of the TF-FGM approach is that the variances for the involved scalars c and z are no more employed for the querying of the look-up table, since it is assumed that the TF formulation is able to take into account properly the turbulence-chemistry interaction. Also, it is worth recalling that NFGM and TF-FGM are employing in this work the same manifold computed at pre-process. This fact means that chemistry is described in the exact same way for both, and it is related to the conditions explored during the manifold computation. The difference between the two approaches stands in how the turbulence effects are taken into account (i.e., β -PDF vs. artificial thickening and wrinkling efficiency function). Although this approach is limited with respect to a standard TF approach with detailed chemistry, some works in the literature have shown its good capability in comparison with more detailed approaches for practical applications [41, 42].

Efficiency Function definition As mentioned the efficiency function is introduced in the equations to recover the effects of the turbulence wrinkling altered during the front thickening procedure. This quantity is defined as the ratio of the flame wrinkling factors for the original flame and the thickened one. Here, E is computed following the formulation given in [19] by Colin et al.:

$$E = \frac{\Xi(\delta_l)}{\Xi(\delta_{TF})} = \frac{1 + \alpha \Gamma \left(\frac{\Delta_e}{\delta_l}, \frac{u'_{\Delta_e}}{s_l} \right) \frac{u'_{\Delta_e}}{s_l}}{1 + \alpha \Gamma \left(\frac{\Delta_e}{\delta_{TF}}, \frac{u'_{\Delta_e}}{s_l} \right) \frac{u'_{\Delta_e}}{s_l}} \quad (4)$$

where in turn:

$$\Gamma \left(\frac{\Delta_e}{\delta_l}, \frac{u'_{\Delta_e}}{s_l} \right) = 0.75 \exp \left[-1.2 / \left(\frac{u'_{\Delta_e}}{s_l} \right)^{0.3} \right] \left(\frac{\Delta_e}{\delta_l} \right)^{2/3} \quad (5)$$

and it stands for the dimensionless stretch of a flame with flame velocity s_l and thickness δ_l submitted to the action of a range of vortices [19]. For the sake of brevity, the other expression is not reported here, since it assumes the exact same form once the laminar flame thickness δ_l is replaced with artificially thickened one δ_{TF} . Furthermore, another important aspect is how the velocity fluctuations at the test filter u'_{Δ_e} are computed. A first attempt can be done considering the subgrid scale turbulent viscosity within the LES model. If the Smagorinsky model is employed for instance, u'_{Δ_e} can be derived as follows:

$$u'_{\Delta_e} = \frac{v_{sgs}}{C_L \Delta} \quad (6)$$

however, as reported in [19], this approach has two main drawbacks concerning the accuracy of the model constant C_L for the scales of interest, and the difficulties when dealing with the influence of thermal expansion. For this reason, in the same work, a similarity assumption has been retained as:

$$u'_{\Delta_e} = OP(\tilde{\mathbf{u}}) \approx |(\tilde{\mathbf{u}} - \hat{\mathbf{u}})| \quad (7)$$

where $\tilde{\mathbf{u}}$ is the velocity field from the LES solution and $\hat{\mathbf{u}}$ is the filtered field at the scale Δ_e . This expression is further manipulated to avoid the use of a test filter, obtaining a final expression requiring a third-order derivative (the interested reader is addressed to the reference work [19]). This last fact could be not trivial when the implementation in a CFD solver is considered. An interesting approach to overcome this issue has been carried out is reported in the work by Durand et al. [43]. Here, the velocity fluctuations are derived from the formulation given originally by Colin [19]: here only the formulation valid for unstructured mesh is reported. Firstly, the scale similarity is written for finite volume approximation. An analog expression with the rotational operator is written as:

$$u'_{\Delta_e} = c \Delta_x |\nabla \times (\tilde{\mathbf{u}} - \hat{\mathbf{u}})| = c \Delta_x |\nabla \times \tilde{\mathbf{u}} - \nabla \times \hat{\mathbf{u}}| \quad (8)$$

Then, the evaluation of the curl of the test filter is achieved by using its linear definition:

$$\hat{\mathbf{u}} = \frac{\sum_k \tilde{\mathbf{u}}_k V_k}{\sum_k V_k} \quad (9)$$

where $\tilde{\mathbf{u}}_k$ and V_k are respectively the velocity vector and volume of each cell surrounding the considered cell and evaluated within the main solver cell loop for each time-step.

In this work, both the definitions from eq. 6 and eq. 8 are employed to evaluate how the velocity fluctuations description impacts the final results: for the sake of clarity, the two different implementations will be referred as TF-FGM-A and TF-FGM-B respectively in the next sections.

NUMERICAL SETUP

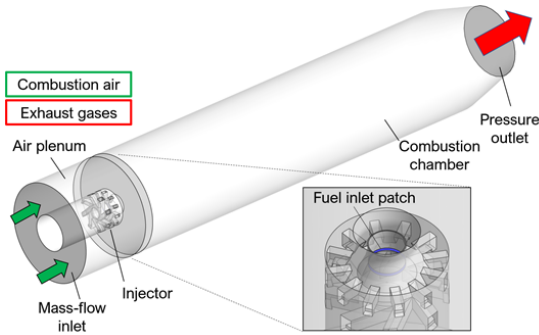


FIGURE 3: NUMERICAL DOMAIN OF THE TEST RIG.

The spatially-filtered compressible Navier-Stokes equations for reactive simulations are solved within LES context, where the subgrid stress tensor has been modeled with the Dynamic Smagorinsky-Lilly model [44]. The numerical schemes employed second-order accuracy for both spatial and temporal discretization. A sketch of the numerical domain is reported in Fig.3, where the flame tube, the nozzle with the related plenum and the convergent outlet are visible. This setup is similar to the one present in a first numerical study conducted by the authors [17] on the same low-swirl injector concept with a smaller effective area: here, the isothermal conditions were studied and reached a good agreement in terms of flow-field description. Indeed the present work focused only on the reactive point, similarly to the study conducted in [18] for evaluating the impact of the turbulent combustion modelling. Thus, it is assumed that the numerical setup can correctly represent the flow structures in absence of reaction.

The spatial discretization is based on an unstructured mesh grid with polyhedral elements. The large extension of the reaction zone comprehensive of the lift-off region means a wide

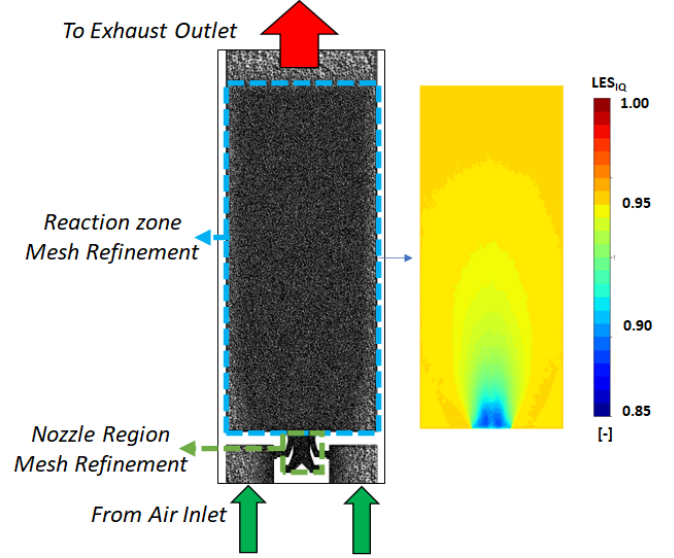


FIGURE 4: MESH GRID ADOPTED IN THE SIMULATIONS AND LES INDEX QUALITY MAP.

volume requiring local refinement. This clearly impacts the computational cost of the simulation and limits the element sizing. A good approach to overcome this issue is reported in the literature through the use of Adaptive Mesh Refinement (AMR), especially if coupled with TF combustion model [45]: the mesh grid is locally refined only where necessary, based on the evaluation of some indicators. In this way, the numerical cost is reduced drastically, while the complexities are due to the handling of the mesh refinement from the parallel computing algorithm. However here the same mesh grid employed in the previous works by the authors is used in order to assess the advantages introduced with the different combustion modelling. Moreover, a detailed discussion of the pro and cons of the AMR method is out of scope and the interested reader is referred to the dedicated literature [46, 47]. The overall number of elements approach 16 M, that has shown to be a good trade-off between accuracy and computational efforts. The refinement regions are two: one within the swirler and the other in the flame tube (see Fig.4). The latter region extends up to 250 mm in the axial direction and to the chamber walls along the radial one, with an element size of $600\mu\text{m}$. A slightly lower sizing is applied within the swirler that is $500\mu\text{m}$ and 5 prismatic layers are used for near-wall treatment. Mesh sensitivity tests have not been carried out at this step and it will be the object of future works. Also, the thickening factor F magnitude within the flame tube has shown an acceptable maximum value of around 7 [30].

At this stage, the adequacy of the calculation grids is evaluated with the LES Quality Index (LES_{IQ}) by Celik et al. [48], where the capability of the mesh grid to properly describe the flow structures is assessed when a value greater or equal to 0.8 is

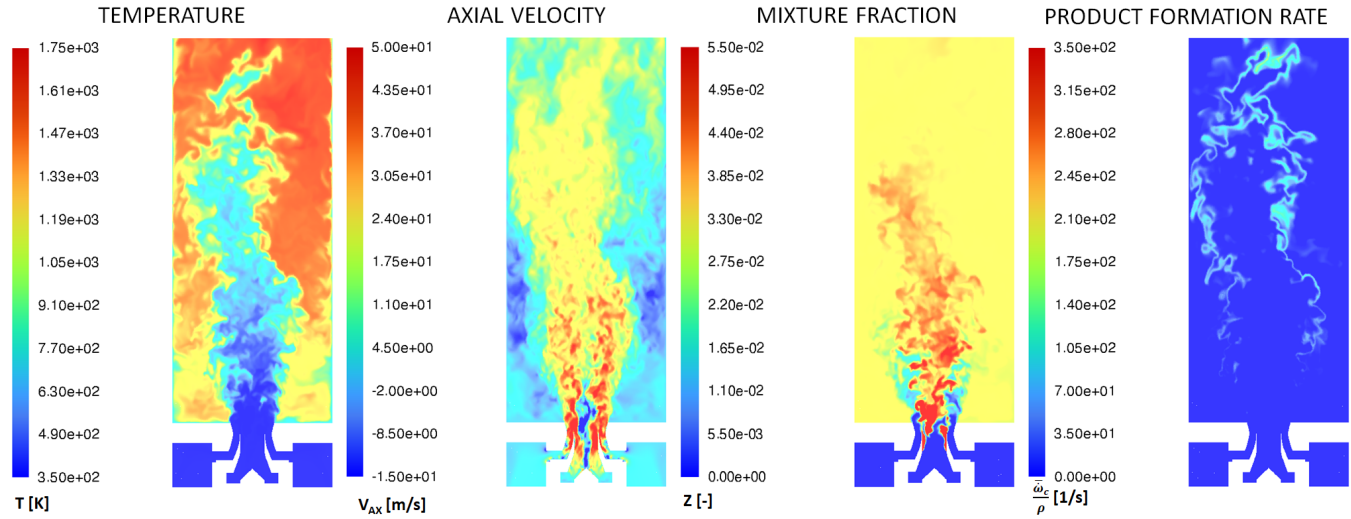


FIGURE 5: INSTANTANEOUS FIELD OF (FROM LEFT TO RIGHT): TEMPERATURE, AXIAL VELOCITY, MIXTURE FRACTION AND PRODUCT FORMATION RATE (I.E., PROGRESS VARIABLE SOURCE TERM OVER DENSITY) FOR THE TF-FGM-A MODEL.

obtained (see Fig.4). This requirement is satisfied in the main reaction zone region, while the minimum value equals 0.7 which is reached at the nozzle outlet section, where turbulent fluctuations are stronger due to the proximity of the swirler.

Concerning the boundary conditions, air mass-flow is imposed to both air and fuel inlets, while the atmospheric pressure is set to the outlet, according to the conditions reported in Tab.1. The fuel is injected with a dedicated inlet patch prior to the prefilmer lip, where its mass flow is derived accordingly to the global equivalence ratio. No-slip condition is applied to the combustion chamber walls and a uniform temperature of 700 K is imposed as thermal boundary condition on the lateral and bottom walls. This point is crucial and it has been largely discussed in [18]. In the previous works, this value of wall temperature seems to better describe the temperature field in the proximity of the combustion chamber bottom walls. Although the use of a uniform temperature with an all in all low magnitude might appear an ill-conceived strategy, this setting has been kept aiming to evaluate the newly tested combustion models with the same setup of the previous works: the consequences of such choice will be discussed in detail in the results section. Indeed, this can be considered a reasonable value considering the GT application field [33,49].

Time step has been set to 3e-06s, with a maximum value of the CFL in the combustion chamber below 5. Each model has a first run to ensure the establishment of the unsteady flow structures in the main reaction zone. Therefore, the averaging is performed for 40 ms, 105 ms and 47 ms respectively for the FGM model, the TF-FGM-A and for the TF-FGM-B.

RESULTS

In this section, the numerical results are compared with the experimental data in terms of the velocity field, local gas composition, CO mole fraction and temperature field. A brief overview of the stabilization mechanism is reported in Fig.5, aiming to better explain how this flame works. Here, the instantaneous contours for the TF-FGM-A simulation are reported in terms of the temperature, axial velocity, mixture fraction, and progress variable source term over density. From the velocity field are clearly visible the swirling jet and the related outer recirculation zone at larger radii. If compared with the temperature field, it is possible to notice the flow instabilities on the outer shear layer which entrains hot combustion products into the main jet, helping the stabilization at lean reactive mixture composition. This fact can be seen also if the mixture fraction field is considered, where $z=0.055$ corresponds to the stoichiometric mixture fraction. The outer recirculation zone is dominated by vitiated products, at the nominal composition of the operating point. Instead, near the burner axis a fuel-rich composition is present initially, while it approaches the nominal value when moving downstream. Finally, the reaction occurs only away from the nozzle outlet and in those regions where a suitable low velocity is reached. This fact could point out a stabilization mechanism similar to the one originally described by Vanquickenborne and Van Tiggelen in [50] for a fully premixed lifted flame, as also suggested in [5]. However, a detailed description of the stabilization mechanism is out of scope and the interested reader is addressed to previous works [17, 18].

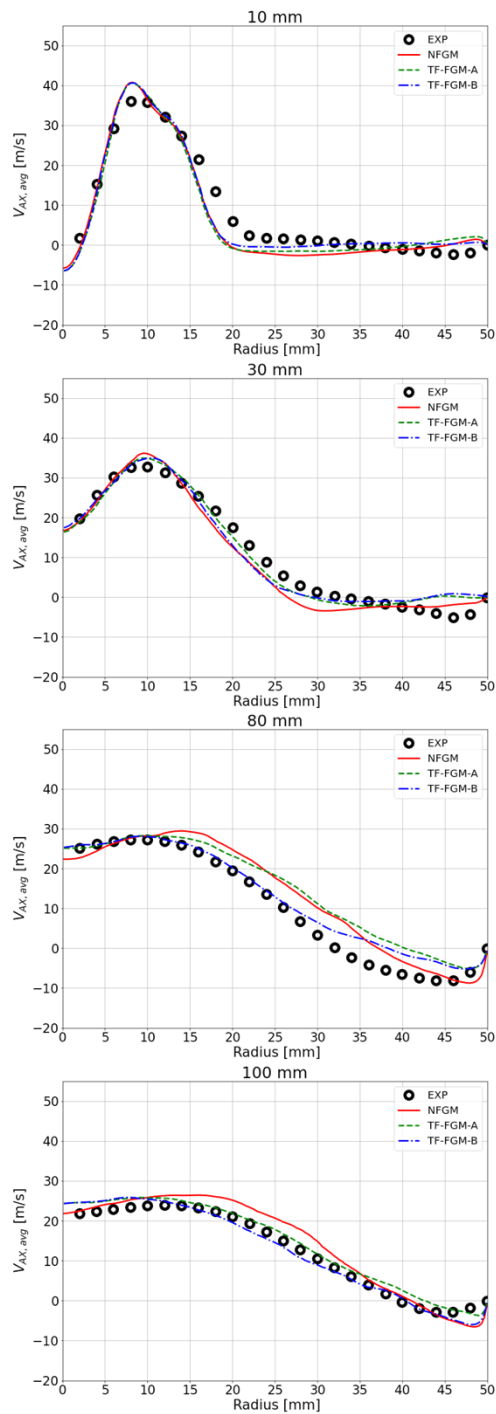


FIGURE 6: RADIAL PROFILES OF MEAN AXIAL VELOCITY AT GIVEN AXIAL POSITIONS FOR ALL THE CFD MODELS, AND EXP ADAPTED FROM [4].

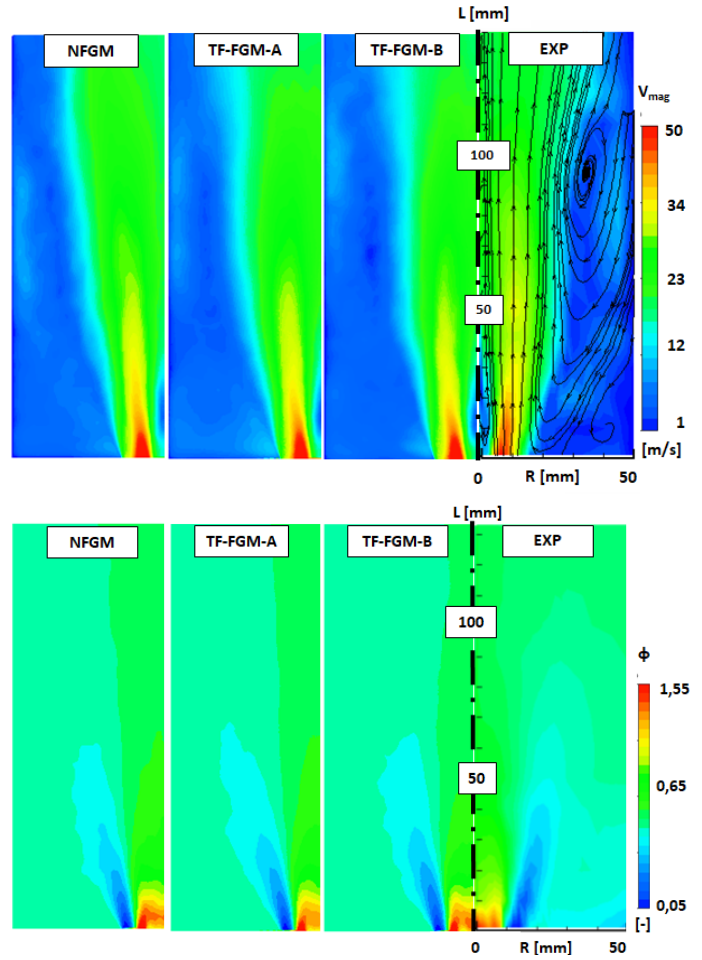


FIGURE 7: COMPARISON CFD-EXP FROM LEFT TO RIGHT: NFGM, TF-FGM-A,TF-FGM-B, AND EXP ADAPTED FROM [4]. TOP: MEAN VELOCITY MAGNITUDE, BOTTOM: MEAN EQUIVALENCE RATIO.

Flow-field and equivalence ratio

A first comparison between numerics and experiments concerns the velocity and equivalence ratio fields. In Fig.6 are reported the mean axial velocity profiles at given axial positions, while in Fig.7 the velocity field on the midplane up to 175 mm is reported for both CFD and experiments in terms of mean velocity magnitude maps. It can be observed that numerical simulations are in good agreement with the experimental data since all the key features are present, regardless of the specific combustion model. That means the high-velocity streams close to the burner axis and rapidly decaying away from it in the radial direction, as well as the short and weak IRZ near the burner axis. Furthermore, the ORZ extends above 100 mm, as reported in the experimental map. As it will be shown later, the NFGM approach tends to reproduce a flame stabilized too low in the combustion

chamber: the early occurrence of the thermal expansion justifies the overestimation of the axial velocity at higher axial distance.

The local composition of the mixture is reported in Fig.7 in terms of equivalence ratio ϕ contour maps. Since methane is injected only in the primary swirler, a fuel-rich composition is present close to the nozzle axis at the nozzle outlet section, as already mentioned. Also, the pure air jets related to the secondary swirler are visible at the bottom of the combustion chamber. The radial channels are indeed responsible for a flow characterized by a very lean mixture and high axial velocity. Therefore, the flame reattachment is avoided, since these flow structures act as a barrier between the recirculating hot gas and the fresh mixture in the inner region. Also in this case, the investigated models are in good agreement with the experimental data from a qualitative point of view. Some discrepancies are present instead considering the field near the bottom of the chamber, which seems with a leaner composition in the experimental contour.

CO mole fraction

The most important quantity among the chemical species measured in [5] is surely the carbon monoxide mole fraction X_{CO} , since it is an indicator of the ongoing reaction from a qualitative point of view. It should be highlighted that the maximum value for X_{CO} is 0.0055 for the experimental contours, while it is around 0.012 for all the numerical models employed here (i.e., NFGM, TF-FGM-A, and TF-FGM-B): the results are presented here in terms of normalized value over the maximum, following the same approach of the previous works. In Fig.8 the contour maps of carbon monoxide mole fraction, X_{CO} are reported for the employed combustion models in this work, other than the outcomes from [18] for the sake of clarity. Firstly, each combustion model is predicting the flame lift-off, since all the maps are showing the reaction zones detached from the nozzle exit. This fact was already noticed also with the standard FGM model with adiabatic flamelets in [18]. As well, each model is predicting the arrow-shaped flame according to the experimental findings with the base anchored on the outer shear layer of the main swirling jet. When the NFGM model is used, the flame appears quite compact and short with respect to the experiments, where the higher values of X_{CO} are found between 125 and 175mm. Compared with the FGM with adiabatic flamelets manifold, it still could be seen as an improvement, since the flame assumes a wider reaction zone. The flame base instead is still anchored at the same height observed with the standard FGM model and generally high values of X_{CO} can be found in the shear layer between ORZ and the nozzle swirling jet.

It should be noticed also that although the manifold takes into account the effects of heat losses thanks to this novel manifold, this situation is verified mainly in the bottom corners of the combustion chamber, as can be seen in Fig.9. The heat loss is defined as $\Delta h = (h - h_{ad})/h_{ad}$ being h the mixture enthalpy and

h_{ad} the adiabatic enthalpy for the given equivalence ratio [38]. The inner core and the mean reaction zone instead are not affected directly but, as observed in the experiments, it has an indirect effect due to the decrease of the recirculating gas temperature, postponing the ignition of the mixture and thus decreasing the reactivity at the flame base. Furthermore, it is worth recalling that the NFGM approach is assuming a simplified model to account for turbulence effects in the enthalpy transport equation through a δ -function, while TF-FGM employs the thickening procedure in this equation, retrieving a better description of such effects. Regarding the β -PDF assumptions for c and z instead, it has been shown in the literature [15] how these could be not fully representative of a modern gas turbine combustor scenario if compared with finite-rate chemistry approaches: the use of TF-FGM approach could possibly help to recover this effect. A good agreement in terms of flame shape and reproduction of the lift-off is instead reached considering the TF-FGM combustion model. The main reaction zone, where the highest value of the X_{CO} is reached is between 100 and 200 mm, which is shown also by the EXP map. Moreover, on the burner axis, CFD and EXP data are almost coincident where the most reactive region begins, which is around 110mm. Instead, the largest differences are still related to an early occurrence of the reaction zone in the lower part of the chamber. This concerns the outer shear layer of the swirling jet, where the flame is anchored, which is showing a non-negligible presence of CO with respect to the EXP data. Furthermore, the use of the most accurate computation of the velocity fluctuation with the TF-FGM-B model predicts better the post-flame region, which appears very close to the experimental data, while the TF-FGM-A model instead presents a larger extension of this region. Nevertheless, such results are showing a strong improvement with respect to the results obtained with other approaches such as the pure TF model with semi-global mechanism where the flame position exceeded the experimental finding.

Temperature field

In Fig.10 the temperature field maps are reported again for all the combustion models and compared with the experimental results. Here, the lift-off distance is visible thanks to the cold region which is present near the burner's axis, in correspondence of the swirling jet. Instead, the ORZ is dominated by the combustion products, being transported here from the flame region. The effects of the different combustion models indeed affect the extension of this cold jet, accordingly to the position of the main reaction zone in the flame tube, as shown in the CO mole fraction maps. However, the temperature field is affected by the assumption made for the thermal boundary condition on the wall, which is a uniform temperature equal to 700K.

The temperature seems fairly well predicted if the bottom corners of the chamber are considered. Also, the flame root (label "1" in

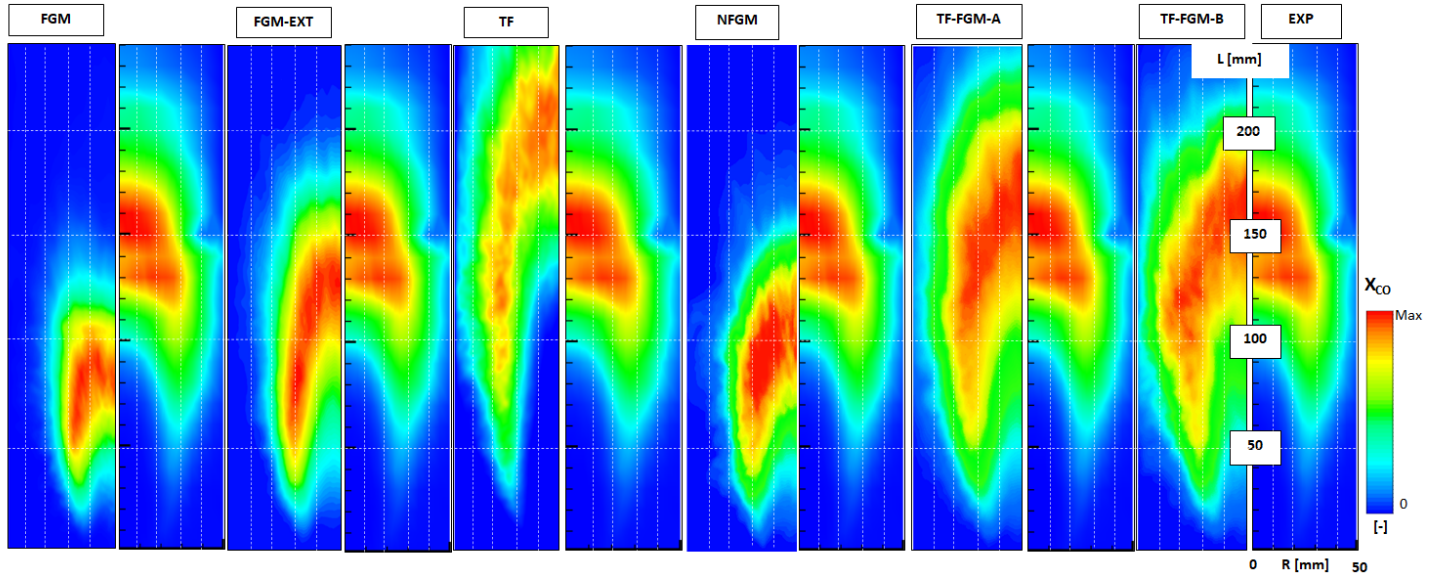


FIGURE 8: MEAN CO MOLE FRACTION MAPS COMPARISON. FROM LEFT TO RIGHT:FGM, FGM-EXT, TF (ADAPTED FROM [18]), NFGM, TF-FGM-A, AND TF-FGM-B. EXP DATA ADAPTED FROM [4] ARE REPORTED ON THE RIGHT SIDE FOR EACH COMPARISON.

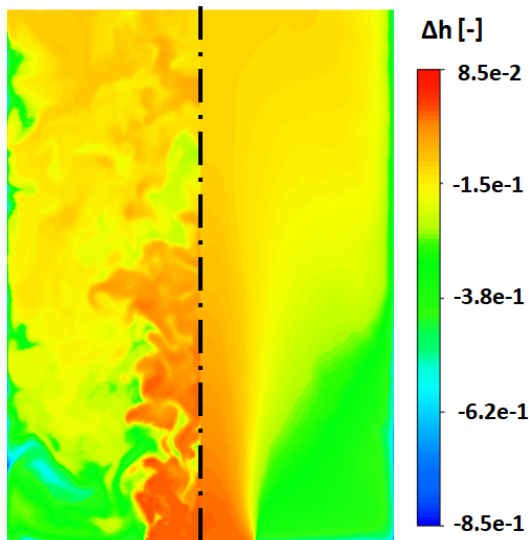


FIGURE 9: HEAT LOSS CONTOUR MAPS UP TO 135 mm COMING FROM THE TF-FGM-A SIMULATION. LEFT: INSTANTANEOUS. RIGHT:MEAN.

Fig. 10) is established near 50 mm in the axial direction, which is very close to the experimental measurement. This means that this assumption could reasonably be representative of the actual wall temperature near the bottom wall. However, assuming this thermal boundary condition also on the lateral confinement wall is leading to a wrong prediction of the temperature field down-

stream of the main reaction zone (label “3” in Fig. 10). This is clear if the NFGM map is considered: although this model has the worst agreement with the CO experimental finding, it also has the best agreement concerning the temperature field. Due to the early occurrence of the reaction zone, the post flame region temperature field is better described with respect to both the TF-FGM models. At the same time, this fact could also explain why the TF-FGM model is predicting a higher level of CO with respect to the experimental measurements, since the finite rate chemistry is slowed down due to the imposed lower temperature. Considering label “2” in Fig. 10, the spread of the flame front is highlighted in the outer shear layer of the swirling jet. This region assumes an intermediate temperature between the fresh mixture and the fully oxidized reaction products. Both TF-FGM-A and TF-FGM-B are quite in agreement with the experimental finding. Here, the TF-FGM-B is expected to have a better agreement, since the more accurate computation of the velocity fluctuations, thus the flame brush in this zone. Nevertheless, these results should be evaluated with a longer averaging for the TF-FGM-B. As well, the prediction of the cold jet penetration is very well predicted reaching the 100 mm of height similar to the EXP map for both the models with the flame thickening.

CONCLUSIONS

The numerical investigation of a low-swirl lifted partially premixed flame operated with gaseous fuel has been carried out with a coupled TF-FGM combustion model. In order to account

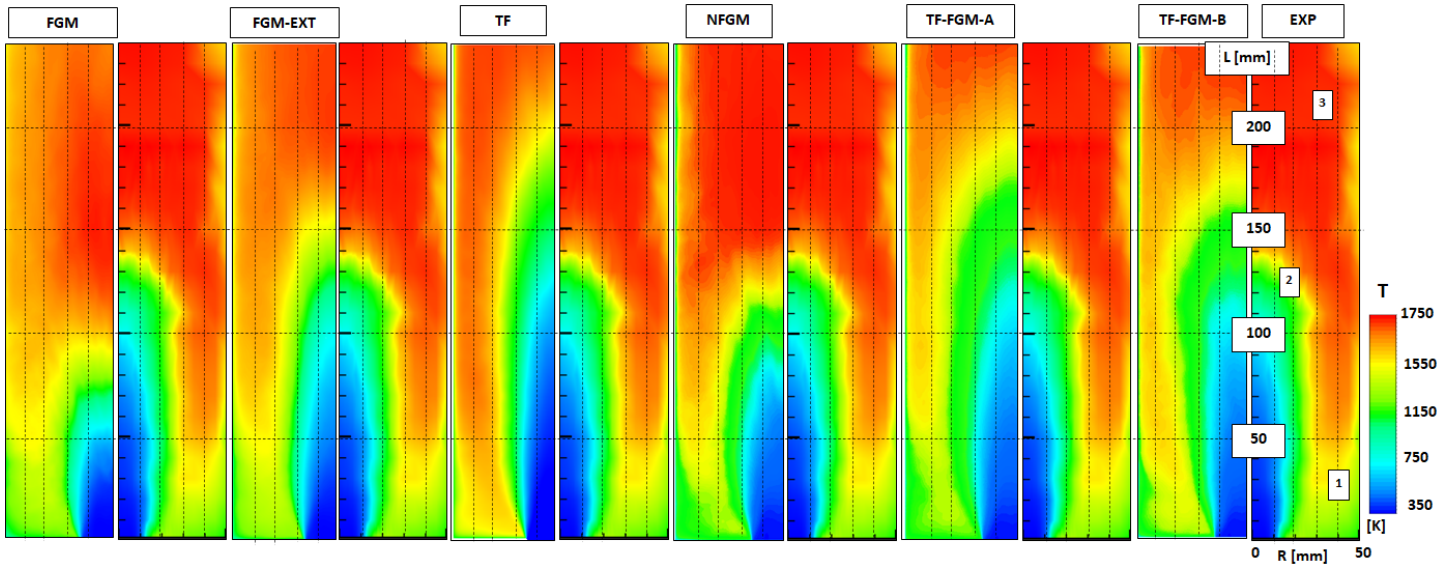


FIGURE 10: MEAN TEMPERATURE FIELD MAPS COMPARISON. FROM LEFT TO RIGHT:FGM, FGM-EXT, TF (ADAPTED FROM [18]), AND TF-FGM-A,TF-FGM-B. EXP DATA ADAPTED FROM [4] ARE REPORTED ON THE RIGHT SIDE FOR EACH COMPARISON.

for heat loss effects on the flame front, as well as possible stratification of the reactive mixture, the look-up table is parametrized as function of various levels of heat loss/gain, other than progress variable and mixture fraction. This work follows an extensive numerical campaign performed recently by the authors on this test case, where FGM (with adiabatic flamelets manifold) and TF were applied singularly, obtaining a not fully satisfactory agreement with experimental data. With respect to this previous work, here, three additional combustion models are employed: FGM with non-adiabatic manifold, and TF-FGM model with two different strategies to compute the velocity fluctuations in the efficiency function. As observed in the first work with standard FGM and TF models, both the flow-field and local composition do not exhibit relevant discrepancies with the experimental data. Concerning the CO fraction field, it is confirmed again that the standard FGM approach is not able to correctly predict the flame lift-off magnitude, although the use of a look-up table generated from non-adiabatic flamelets brings some slight improvements with respect of the previous works. The introduction of the coupled TF-FGM model results in a better prediction of the flame shape and lift-off, especially considering the main reaction zone position. Further improvements can be obtained depending on how the velocity fluctuations at the test filter in the efficiency function are computed. Here, the use of a more accurate formulation leads to a better shape with respect to the computation from the subgrid model employed in the LES simulations. A limit within the present study is due to the use of a uniform wall temperature, as in the previous studies. Concerning the temperature field, further improvements are expected if a more represen-

tative boundary condition for the wall temperature is employed. Also, it should be noticed that this step is particularly challenging due to the limited information on this aspect of the test rig. In conclusion, the outcomes of this study can be summarized as follows:

1. The inclusion of the heat losses effects within the FGM context, per se, is not enough to reproduce correctly the flame, at least for this test case.
2. The advantages of the TF-FGM approach consist in a different description of the turbulence-chemistry interaction, with respect to β -shaped PDF used for the standard FGM model. Also, it should be noticed that the TF-FGM approach introduces the effects of the turbulence also for the enthalpy equation, while the current implementation of the NFGM adopts a simplified description. These advantages could be affected when a more refined mesh is employed, hence when the contribution of the sub-grid scales is reduced until it becomes negligible.
3. The computational efforts for the three approaches employed here are comparable, while a better representation of the flame is obtained with the TF-FGM approach. This fact is particularly appealing considering industrial applications or more complex burner configurations.

Another interesting point could be to explore the influence of different formulations of the efficiency function for the turbulence effects. Finally, the manifold here employed takes into account only for the heat loss, but indeed also the action of the stretch on the flame front could be relevant and its impact should be inves-

tigated.

ACKNOWLEDGMENT

This project has received funding from the Clean Sky 2 Joint Undertaking (JU) under grant agreement N. 831881 (CHAIr-LIFT). The JU receives support from the European Union's Horizon 2020 research and innovation program and the Clean Sky 2 JU members other than the Union.



The authors acknowledge the CINECA award under the IS-CRA initiative, for the availability of high-performance computing resources.

REFERENCES

- [1] Mansouri, Z., Aouissi, M., and Boushaki, T., 2016. "A numerical study of swirl effects on the flow and flame dynamics in a lean premixed combustor". *International journal of heat and technology*, **34**(2), pp. 227–235.
- [2] Cheng, R., Yegian, D., Miyasato, M., Samuelsen, G., Benson, C., Pellizzari, R., and Loftus, P., 2000. "Scaling and development of low-swirl burners for low-emission furnaces and boilers". *Proceedings of the Combustion Institute*, **28**(1), pp. 1305–1313.
- [3] Nogenmyr, K.-J., Bai, X., Petersson, P., Brackman, C., Seyfried, H., Olofsson, J., Sedarsky, D., Alden, M., Linne, M., and Nauert, A., 2006. "Experiments and large eddy simulation in a low swirl burner".
- [4] Fokaides, P., and Zarzalis, N., 2007. "Lean blowout dynamics of a lifted stabilized, non-premixed swirl flame". In *Proceedings of European Combustion Meeting*, Vol. 7, p. 2.
- [5] Fokaides, P. A., Kasabov, P., and Zarzalis, N., 2008. "Experimental investigation of the stability mechanism and emissions of a lifted swirl nonpremixed flame". *Journal of engineering for gas turbines and power*, **130**(1).
- [6] Pitsch, H., Desjardins, O., Balarac, G., and Ihme, M., 2008. "Large-eddy simulation of turbulent reacting flows". *Progress in Aerospace Sciences*, **44**(6), pp. 466–478.
- [7] Gicquel, L. Y., Staffelbach, G., and Poinso, T., 2012. "Large eddy simulations of gaseous flames in gas turbine combustion chambers". *Progress in energy and combustion science*, **38**(6), pp. 782–817.
- [8] Lawn, C., 2009. "Lifted flames on fuel jets in co-flowing air". *Progress in Energy and Combustion Science*, **35**(1), pp. 1–30.
- [9] Maas, U., and Pope, S. B., 1992. "Simplifying chemical kinetics: intrinsic low-dimensional manifolds in composition space". *Combustion and flame*, **88**(3-4), pp. 239–264.
- [10] Pierce, C. D., and Moin, P., 2004. "Progress-variable approach for large-eddy simulation of non-premixed turbulent combustion". *Journal of fluid Mechanics*, **504**, pp. 73–97.
- [11] Van Oijen, J., Lammers, F., and De Goey, L., 2001. "Modeling of complex premixed burner systems by using flamelet-generated manifolds". *Combustion and Flame*, **127**(3), pp. 2124–2134.
- [12] Gicquel, O., Darabiha, N., and Thévenin, D., 2000. "Laminar premixed hydrogen/air counterflow flame simulations using flame prolongation of ildm with differential diffusion". *Proceedings of the Combustion Institute*, **28**(2), pp. 1901–1908.
- [13] Ma, P. C., Wu, H., Labahn, J. W., Jaravel, T., and Ihme, M., 2019. "Analysis of transient blow-out dynamics in a swirl-stabilized combustor using large-eddy simulations". *Proceedings of the Combustion Institute*, **37**(4), pp. 5073–5082.
- [14] Gonzalez-Juez, E. D., Kerstein, A. R., Ranjan, R., and Menon, S., 2017. "Advances and challenges in modeling high-speed turbulent combustion in propulsion systems". *Progress in Energy and Combustion Science*, **60**, pp. 26–67.
- [15] Panchal, A., Ranjan, R., and Menon, S., 2019. "A comparison of finite-rate kinetics and flamelet-generated manifold using a multiscale modeling framework for turbulent premixed combustion". *Combustion Science and Technology*, **191**(5-6), pp. 921–955.
- [16] Kern, M., Fokaides, P., Habisreuther, P., and Zarzalis, N., 2009. "Applicability of a flamelet and a presumed jpdf 2-domain-1-step-kinetic turbulent reaction model for the simulation of a lifted swirl flame". In *Turbo Expo: Power for Land, Sea, and Air*, Vol. 48838, pp. 359–368.
- [17] Langone, L., Sedlmaier, J., Nassini, P. C., Mazzei, L., Harth, S., and Andreini, A., 2020. "Numerical modeling of gaseous partially premixed low-swirl lifted flame at elevated pressure". In *Turbo Expo: Power for Land, Sea, and Air*, Vol. 84133, American Society of Mechanical Engineers, p. V04BT04A068.
- [18] Langone, L., Amerighi, M., and Andreini, A., 2022. "Large eddy simulations of a low-swirl gaseous partially premixed lifted flame in presence of wall heat losses". *Energies*, **15**(3), p. 788.
- [19] Colin, O., Ducros, F., Veynante, D., and Poinso, T., 2000. "A thickened flame model for large eddy simulations of turbulent premixed combustion". *Physics of fluids*, **12**(7), pp. 1843–1863.
- [20] Franzelli, B., Riber, E., Gicquel, L. Y., and Poinso, T., 2012. "Large eddy simulation of combustion instabilities in a lean partially premixed swirled flame". *Combustion*

- and flame, *159*(2), pp. 621–637.
- [21] Franzelli, B. G., 2011. “Impact of the chemical description on direct numerical simulation and large eddy simulation of turbulent combustion in industrial aero-engines”. PhD thesis, Institut National Polytechnique de Toulouse-INPT.
- [22] Jella, S., Kwong, W., Steinberg, A., Park, J., Lu, T., Bergthorson, J., and Bourque, G., 2021. “Attached and lifted flame stabilization in a linear array of swirl injectors”. *Proceedings of the Combustion Institute*, **38**(4), pp. 6279–6287.
- [23] Kuenne, G., Ketelheun, A., and Janicka, J., 2011. “LES modeling of premixed combustion using a thickened flame approach coupled with fgm tabulated chemistry”. *Combustion and Flame*, **158**(9), pp. 1750–1767.
- [24] Proch, F., and Kempf, A. M., 2014. “Numerical analysis of the cambridge stratified flame series using artificial thickened flame les with tabulated premixed flame chemistry”. *Combustion and Flame*, **161**(10), pp. 2627–2646.
- [25] Dressler, L., Sacomano Filho, F., Sadiki, A., and Janicka, J., 2021. “Influence of thickening factor treatment on predictions of spray flame properties using the atf model and tabulated chemistry”. *Flow, Turbulence and Combustion*, **106**(2), pp. 419–451.
- [26] Dressler, L., Ries, F., Kuenne, G., Janicka, J., and Sadiki, A. “Characterization of the stratification process in a turbulent premixed flame using les”.
- [27] Proch, F., and Kempf, A., 2015. “Modeling heat loss effects in the large eddy simulation of a model gas turbine combustor with premixed flamelet generated manifolds”. *Proceedings of the combustion institute*, **35**(3), pp. 3337–3345.
- [28] Lefebvre, A. H., and Ballal, D. R., 2010. *Gas turbine combustion: alternative fuels and emissions*. CRC press.
- [29] Van Oijen, J., Donini, A., Bastiaans, R., ten Thije Boonkkamp, J., and De Goey, L., 2016. “State-of-the-art in premixed combustion modeling using flamelet generated manifolds”. *Progress in Energy and Combustion Science*, **57**, pp. 30–74.
- [30] Poinot, T., and Veynante, D., 2005. *Theoretical and numerical combustion*. RT Edwards, Inc.
- [31] Bilger, R., 1989. “The structure of turbulent nonpremixed flames”. In Symposium (International) on Combustion, Vol. 22, Elsevier, pp. 475–488.
- [32] Fiorina, B., Baron, R., Gicquel, O., Thevenin, D., Carpentier, S., and Darabiha, N., 2003. “Modelling non-adiabatic partially premixed flames using flame-prolongation of ildm”. *Combustion Theory and Modelling*, **7**(3), p. 449.
- [33] Donini, A., Bastiaans, R., Van Oijen, J., and De Goey, L., 2017. “A 5-d implementation of fgm for the large eddy simulation of a stratified swirled flame with heat loss in a gas turbine combustor”. *Flow, turbulence and combustion*, **98**(3), pp. 887–922.
- [34] Gövert, S., Mira, D., Kok, J. B., Vázquez, M., and Houzeaux, G., 2018. “The effect of partial premixing and heat loss on the reacting flow field prediction of a swirl stabilized gas turbine model combustor”. *Flow, turbulence and combustion*, **100**(2), pp. 503–534.
- [35] Tang, Y., and Raman, V., 2021. “Large eddy simulation of premixed turbulent combustion using a non-adiabatic, strain-sensitive flamelet approach”. *Combustion and Flame*, **234**, p. 111655.
- [36] Nunno, A. C., Grenga, T., and Mueller, M. E., 2019. “Comparative analysis of methods for heat losses in turbulent premixed flames using physically-derived reduced-order manifolds”. *Combustion Theory and Modelling*, **23**(1), pp. 42–66.
- [37] ANSYS, 2021. *Fluent 21.2 Theory Guide*.
- [38] Yadav, R., Verma, I., Modak, A., and Li, S., 2020. “A fully non-adiabatic flamelet generated manifold model for high fidelity modeling of turbulent combustion in gas turbine like conditions”. In Turbo Expo: Power for Land, Sea, and Air, Vol. 84133, American Society of Mechanical Engineers, p. V04BT04A026.
- [39] Williams, F., 1985. “Combustion theory: the fundamental theory of chemically reacting flow systems. benjamin/cummings pub. co”.
- [40] Legier, J.-P., Poinot, T., and Veynante, D., 2000. “Dynamically thickened flame les model for premixed and non-premixed turbulent combustion”. In Proceedings of the summer program, Vol. 12, Citeseer.
- [41] Fiorina, B., Mercier, R., Kuenne, G., Ketelheun, A., Avdić, A., Janicka, J., Geyer, D., Dreizler, A., Alenius, E., Duwig, C., et al., 2015. “Challenging modeling strategies for les of non-adiabatic turbulent stratified combustion”. *Combustion and Flame*, **162**(11), pp. 4264–4282.
- [42] Gruhlke, P., Proch, F., Kempf, A. M., Dederichs, S., Beck, C., and Mahiques, E. I., 2018. “Prediction of co and nox pollutants in a stratified bluff body burner”. *Journal of Engineering for Gas Turbines and Power*, **140**(10).
- [43] Durand, L., and Polifke, W., 2007. “Implementation of the thickened flame model for large eddy simulation of turbulent premixed combustion in a commercial solver”. In Turbo Expo: Power for Land, Sea, and Air, Vol. 47918, pp. 869–878.
- [44] Lilly, D. K., 1992. “A proposed modification of the germano subgrid-scale closure method”. *Physics of Fluids A: Fluid Dynamics*, **4**(3), pp. 633–635.
- [45] Mehl, C., Liu, S., and Colin, O., 2021. “A strategy to couple thickened flame model and adaptive mesh refinement for the les of turbulent premixed combustion”. *Flow, Turbulence and Combustion*, **107**(4), pp. 1003–1034.
- [46] Gao, X., and Groth, C., 2006. “A parallel adaptive mesh refinement algorithm for predicting turbulent non-premixed combusting flows”. *International Journal of Computational Fluid Dynamics*, **20**(5), pp. 349–357.
- [47] Bell, J., and Day, M., 2011. “Adaptive methods for simu-

- lation of turbulent combustion”. In *Turbulent Combustion Modeling*. Springer, pp. 301–329.
- [48] Celik, I., Cehreli, Z., and Yavuz, I., 2005. “Index of resolution quality for large eddy simulations”.
- [49] Massey, J. C., Chen, Z. X., and Swaminathan, N., 2021. “Modelling heat loss effects in the large eddy simulation of a lean swirl-stabilised flame”. *Flow, Turbulence and Combustion*, **106**(4), pp. 1355–1378.
- [50] Vanquickenborne, L., and Van Tiggelen, A., 1966. “The stabilization mechanism of lifted diffusion flames”. *Combustion and Flame*, **10**(1), pp. 59–69.